

# Fast classification scheme for HARDI data simplification

Prckovska, V.; Vilanova Bartroli, A.; Poupon, C.; ter Haar Romenij, B.M.; Descoteaux, M.

*Published in:*  
ICT Innovations 2009 part 2

*DOI:*  
[10.1007/978-3-642-10781-8\\_36](https://doi.org/10.1007/978-3-642-10781-8_36)

Published: 01/01/2010

*Document Version*  
Publisher's PDF, also known as Version of Record (includes final page, issue and volume numbers)

## **Please check the document version of this publication:**

- A submitted manuscript is the author's version of the article upon submission and before peer-review. There can be important differences between the submitted version and the official published version of record. People interested in the research are advised to contact the author for the final version of the publication, or visit the DOI to the publisher's website.
- The final author version and the galley proof are versions of the publication after peer review.
- The final published version features the final layout of the paper including the volume, issue and page numbers.

[Link to publication](#)

*Citation for published version (APA):*  
Prckovska, V., Vilanova, A., Poupon, C., Haar Romenij, ter, B. M., & Descoteaux, M. (2010). Fast classification scheme for HARDI data simplification. In D. Davcev, & J. Marx Gómez (Eds.), ICT Innovations 2009 part 2. (pp. 345-355). Berlin Heidelberg: Springer. DOI: 10.1007/978-3-642-10781-8\_36

## **General rights**

Copyright and moral rights for the publications made accessible in the public portal are retained by the authors and/or other copyright owners and it is a condition of accessing publications that users recognise and abide by the legal requirements associated with these rights.

- Users may download and print one copy of any publication from the public portal for the purpose of private study or research.
- You may not further distribute the material or use it for any profit-making activity or commercial gain
- You may freely distribute the URL identifying the publication in the public portal ?

## **Take down policy**

If you believe that this document breaches copyright please contact us providing details, and we will remove access to the work immediately and investigate your claim.

# Fast classification scheme for HARDI data simplification

V. Prčkovska<sup>1</sup>, A. Vilanova<sup>1</sup>, C. Poupon<sup>2</sup>,  
B.M. ter Haar Romeny<sup>1</sup>, and M. Descoteaux<sup>2</sup>

<sup>1</sup> Dept. of Biomedical Engineering, Eindhoven Univ. of Technology, The Netherlands

email: {V.Prckovska, A.Vilanova, B.M.terHaarRomeny}@tue.nl,

<sup>2</sup> NeuroSpin, CEA Saclay, France

email: maxime.descoteaux@gmail.com

**Abstract.** High angular resolution diffusion imaging (HARDI) is able to capture the water diffusion pattern in areas of complex intravoxel fiber configurations. However, compared to diffusion tensor imaging (DTI), HARDI adds extra complexity (e.g., high post-processing time and memory costs, nonintuitive visualization). Separating the data into Gaussian and non-Gaussian areas can allow to use complex HARDI models just when it is necessary. We study HARDI anisotropy measures as classification criteria applied to different HARDI models. The chosen measures are fast to calculate and provide interactive data classification. We show that increasing b-value and number of diffusion measurements above clinically accepted settings does not significantly improve the classification power of the measures. Moreover, denoising enables better quality classifications even with low b-values and low sampling schemes. We study the measures quantitatively on an ex-vivo crossing phantom, and qualitatively on real data under different acquisition schemes.

**Keywords:** High Angular Resolution Diffusion Imaging, Diffusion Tensor Imaging, Diffusion Weighted Magnetic Resonance Imaging, voxel classification, HARDI, DTI, DW-MRI

## 1 Introduction

Diffusion tensor imaging (DTI) is a recent technique that can map the orientation architecture of neural tissues in a completely non-invasive way by measuring the directional specificity (anisotropy) of local water diffusion [1]. The diffusion tensor model however, has well known limitations in areas of complex intravoxel heterogeneity with crossing fibers, where the diffusion process can not be modeled as Gaussian. Nonetheless, DTI is still very popular and has many advantages like: fast and clinically feasible acquisition schemes (typically 7-60 number of gradients (NG), b-values  $1000 \text{ s/mm}^2$  and total acquisition time of 3-5 minutes), fast post-processing of the data that allows interactivity in the data exploration, simple visualization techniques and modeling using well-developed tensor mathematics. To overcome the limitations of DTI, more sophisticated models were introduced using high angular resolution diffusion (HARDI). For HARDI, about sixty to a several hundred diffusion gradients are acquired in

order to reconstruct certain spherical probability functions (SPFs) that either recover the underlying fiber populations or depict certain diffusion properties. Popular HARDI reconstruction techniques include ADC modeling [2, 3], QBall imaging [4], diffusion orientation transform (DOT) [5], spherical deconvolution (SD) [6], and several other model-based methods. The produced output by the above techniques is always given in the form of a spherical function  $\psi(\theta, \phi)$  that characterizes the local intra-voxel fiber structure. This function can be represented using spherical harmonics (SH)

$$\psi(\theta, \phi) = \sum_{l=0}^{l_{max}} \sum_{m=-l}^l a_l^m Y_l^m(\theta, \phi), \quad (1)$$

where  $Y_l^m$  represent the spherical harmonics of order  $l$  and phase  $m$ , and  $l_{max}$  is the truncation order of the SH series.

HARDI has obvious advantages over DTI in crossing configurations, but has several drawbacks that come along with this complex modeling: longer processing time of the data (that can typically take few hours to a few days), inability to interactively explore the data because of over-cluttered and computationally heavy visualization as well as longer data acquisitions. Hence, one wonders if a complex high-order modeling of the data is always needed (i.e. at every voxel) or worths its drawbacks? In crossing areas, it is certainly justified, but for a large part of the white matter, there are significant single fiber voxels where high-order modeling might be redundant. Being able to classify regions of single fiber (Gaussian) and crossing fibers (non-Gaussian) in white matter in a fast and reliable way, is thus important. It can reduce the modeling complexity in areas where it is not needed enabling possibilities for data simplification that has many advantages for further post-processing and visualization of the data, especially w.r.t. reducing the computer memory requirements. This will undoubtedly make HARDI data easier to manipulate and interact with, making it more attractive for clinical applications.

There is a wide range of anisotropy measures proposed in literature, such as [2–4, 7–11]. Several authors [3, 8, 9] have attempted to use some of these methods to classify non-Gaussian profiles, but all these attempts have been made on the apparent diffusion coefficient (ADC) profiles and without convincing real data results. In this paper, we explore and compare the classification power of these measures, and apply them on several different SPFs represented in SH basis. We also extract the number of maxima from the corresponding glyph representations. To illustrate the possible application of our data simplification from the classification output, we evaluate the gain in speed for calculation of  $8^{th}$  order constrained spherical deconvolution (CSD) [12] only in non-Gaussian areas and  $2^{nd}$  order ODFs calculated from diffusion tensors in Gaussian areas, compared to only use of  $8^{th}$ -order CSD everywhere in the real data. An important contribution is that we study the classification measures under different b-values and sampling scheme acquisitions from several real HARDI datasets. We also validate the classification experiments on an *ex vivo* phantom with known ground truth. We thus come to several conclusions suggesting that HARDI processing and data interaction are possible in clinical settings.

## 2 Methods

We implemented several anisotropy measures from the literature, generalized anisotropy (GA) [10], generalized fractional anisotropy (GFA) [4], the Shannon entropy (SE) of [11], the cumulative residual entropy (CRE) of [7, 8], as well as fractional multifiber index (FMI) [2], and  $R_0$ ,  $R_2$ ,  $R_i$  [9]. These measures were applied on the ADC profiles [2, 3], analytical QBalls [13] and the DOT [5]. The DOT generally produces much sharper glyph profiles for high  $R_0$  value at the cost of more noisy profiles with spurious peaks. Finding the *best*  $R_0$  in real data is difficult and often done by observation [5]. Hence, to avoid this  $R_0$  selection problem and inspired by definitions of the ODF from q-ball imaging [4] and the marginal ODF (mODF) from diffusion spectrum imaging (DSI) [14], we propose the similar ODFs computed from the DOT as:

$$\psi_{\text{DOT-ODF}}(\theta, \phi) = \int_0^{R_{0max}} P(r, \theta, \phi) dr, \quad \psi_{\text{DOT-mODF}} = \int_0^{R_{0max}} P(r, \theta, \phi) r^2 dr, \quad (2)$$

where  $P(r, \theta, \phi)$  is the probability density function (PDF) computed from DOT [5], and  $R_{0max}$  is set to a conservatively high value (as an example see table on Figure 1).

As a discrete binary measure for classification we propose to use the number of maxima (NM). NM uses the number of local maxima of the min-max normalized SPFs profiles, where the discrete spherical function surpasses a certain threshold (here, we use 0.6) from points on a fine discrete mesh. Moreover, for better visual perception, in our figures we generate min-max normalized RGB color coded glyphs, although one must keep in mind that this normalization enhances angular contrast of glyphs in the white matter but also deforms isotropic glyphs considerably.

**Diffusion Data Acquisition *Ex-vivo* phantom:** To test our classification measures, we use two real physical *ex-vivo* phantoms with fibre bundles crossing at  $45^\circ$  and  $90^\circ$  [15]. These datasets serve as ground truth, where the number of crossing and linear voxels is known. The phantom data was acquired on a 1.5T Signa MR system (GE Healthcare), TE/TR = 130ms/4.5s, 12.0s ( $45^\circ$  and  $90^\circ$  phantom, respectively), BW=200KHz. We analyze the data acquired at two b-values of  $b = 2000$  and  $b = 8000$  s/mm<sup>2</sup>, along 200 uniform directions.

**Human:** Diffusion acquisitions were performed using a twice focused spin-echo echo-planar imaging sequence on a Siemens Allegra 3T scanner, with FOV  $208 \times 208$  mm, isotropic voxels of 2mm. Uniform gradient direction schemes with 49 and 121 directions were used and the diffusion-weighted volumes were interleaved with  $b_0$  volumes every 12th scanned gradient direction. Datasets were acquired at b-values of 1000, 1500, 2000, 3000, 4000 s/mm<sup>2</sup> and in the same session, two anatomical data sets (192 slices, isotropic 1mm voxels) were acquired using the ADNI protocol for registration. Finally, before HARDI reconstruction of the ADC, QBalls and DOT, we applied a denoising pre-processing step [16], available [online](http://www.irisa.fr/visages/benchmarks/)<sup>1</sup>, to correct for the Rician noise bias in the datasets.

<sup>1</sup> <http://www.irisa.fr/visages/benchmarks/>

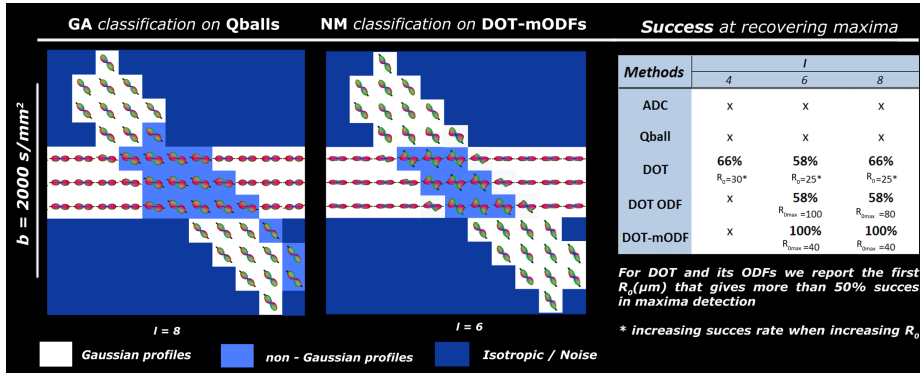
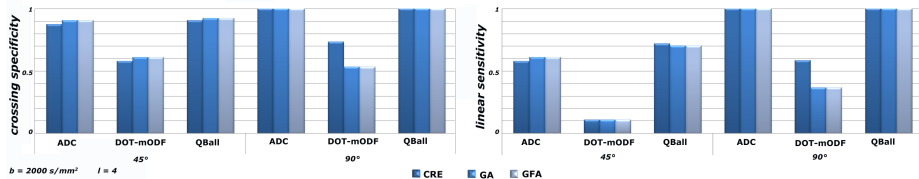


Fig. 1. Classification results from the phantom data.

### 3 Results

**Phantom Results** The  $45^\circ$  is a challenging angle where most of the HARDI techniques struggle to detect multiple maxima, especially at low b-values. We will first analyze the results from the maxima detection. As pointed in the work of Prckovska et al. [17], DOT has the potential of recovering small angles regardless of the b-value, which we demonstrate in the table of Figure 1. In the table we report the success at recovering two maxima in the crossing voxels by all of the examined SPFs. We additionally report the first  $R_0$  for the DOT and its derivations at which the success is greater than 50%. Even more interesting, we observe that the derivation of the DOT discussed in Section 2, with its ODFs (DOT-ODF and DOT-mODF) manifest similar behavior as the DOT itself, which show a better angular resolution than QBall and suggest a better choice of reconstruction algorithm for fiber tracking purpose. The results from the NM classification on the  $90^\circ$  phantom are omitted, due to the 100% success demonstrated in all reconstruction methods.

For the rest of the anisotropy measures we can quantitatively describe the classification power of the  $45^\circ$  and  $90^\circ$  phantoms by using binary classification statistical test. We thus report the specificity and sensitivity of the classified crossing and linear voxels respectively. The sensitivity measures the proportion of actual positives which are correctly identified as such, and the specificity measures the proportion of negatives which are correctly identified. All the measures must be thresholded to obtain the classification and this process is sensitive. Two thresholds are needed to separate the interval of anisotropy values into three distinct compartments: Isotropic/noise, Gaussian and non-Gaussian. We thus iterate over the whole range of values of each anisotropy measure and find the interval where all the crossings are detected while the number of false positives stays minimal. For the purpose of data simplification, it is very dangerous the presence of false negatives (i.e. crossings detected as linear), because relevant information can be lost. Therefore to ensure absence of false negatives we set the sensitivity of crossing classification criteria to 1. In other words, we ensure that all the crossings voxels are always detected (*crossing sensitivity* = 1) and no crossing voxel is classified as linear (*linear specificity* = 1). In Figure 2, we



**Fig. 2.** Specificity and sensitivity demonstrated for the crossing and linear areas in the phantoms respectively.

present the specificity of the crossing classification for each measure and the sensitivity of the linear detected voxels for the 45° and 90° phantoms respectively. Any measure with high specificity is a good candidate for classifying the crossing regions.

We observe that all the three measures CRE, GA and GFA demonstrate similar classification power applied on ADC and QBall profiles. The DOT-mODF however (and similar DOT and DOT-ODF), is substantially worse, even though it produces sharper angular profiles. The sharper and thus, more spiky DOT profiles, are actually a disadvantage for classification measures, as they then produce many false positives in the linear voxels part of the branches of the phantom. Another important result is that increasing the order of SH representation does not significantly improve the classification power of the measures. The results coincide for the sensitivity of the linear classification. The other measures  $FMI$ ,  $R_0$ ,  $R_2$  and  $R_i$ , demonstrate more irregularities and dependencies on the angular configuration of the crossing diffusion pattern and it was more difficult to find thresholds for classification. They were thus omitted in the tables but it is worth mentioning that they did improve at higher b-value when tested in the phantom dataset at  $b = 8000s/mm^2$ . Shannon entropy however, was impossible to threshold with our criteria and was omitted from the analysis. Therefore, from our *ex-vivo* phantom study, we can conclude that CRE, GA and GFA can be applied as a reliable classification between Gaussian and non-Gaussian profiles with in general less than 8% false positive classification results in any configuration. GA and GFA have advantage over CRE since they can be calculated only on the SH coefficients and therefore are significantly faster. Moreover, an SH order of 4 is sufficient to classify the non-Gaussian profiles. However, if one is interested in the number of maxima, it is then useful to use higher SH order to discriminate low angle crossings, such as 45°.

**Human Data Results** The centrum semiovale was used to illustrate the qualitative analysis of the classification results. It is an interesting region for analysis, since fibers of the corpus callosum (CC), corticospinal tract (CST), and superior longitudinal fasciculus (SLF) form different two-fiber and three-fiber crossing configurations in that area. The region-of-interest (ROI) was defined on a coronal slice (Figure 3a). It is important to mention that all the real data results are from similar regions, since those are different HARDI scans from the same subject, and have not been registered. We applied the same classification measures as for the phantom study on the original and denoised data from our datasets. Denoising dramatically improves the glyph profiles and the coherence

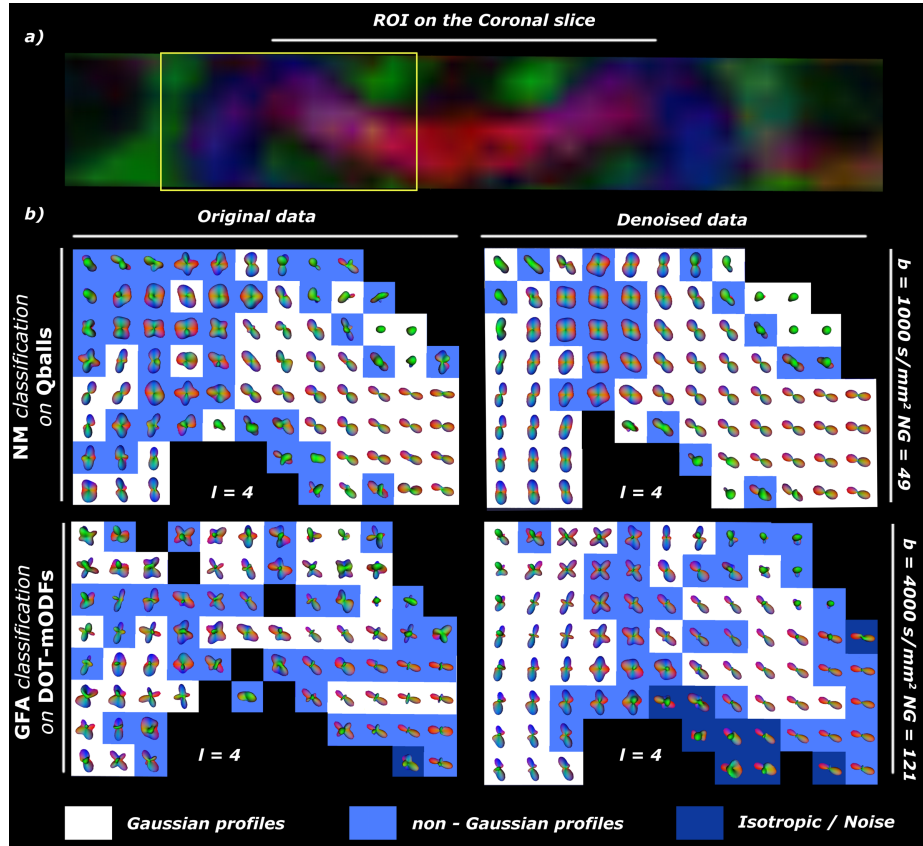


**Fig. 3.** The effect of denoising demonstrated on original versus denoised data in different acquisition schemes

of the non-Gaussian regions, as seen in Figure 3. We also observe a decrease in the irregularities in the crossing profiles. Our results suggest that even at low  $b$ -value, low NG and low estimation SH order, there is success in recovering crossing diffusion patterns and identifying linear regions. In opposite, going to very high  $b$ -values (i.e.  $\geq 3000 \text{ s/mm}^2$ ) and modeling the data with high SH order ( $\geq 6$ ) results in polluted glyphs regardless with or without a denoising phase. Comparing the results of the classification from different measures, we observe that increasing the  $b$ -value sharpens the HARDI profiles and benefits only for maxima extraction purposes. However, there is no significant gain in classification of non-Gaussian profiles, as observed in the phantom study. This is seen in Figure 4, where we see sharper glyphs for DOT-mODF but similar classification power regardless the measure or acquisition scheme. We also note that increasing the model order ( $l > 4$ ) does not increase the classification power. This leads to the conclusion that 49 directions is sufficient for recovering most of the crossings and non-Gaussian voxel detection, which can significantly reduce acquisition time (compared to a 121 NG acquisition).

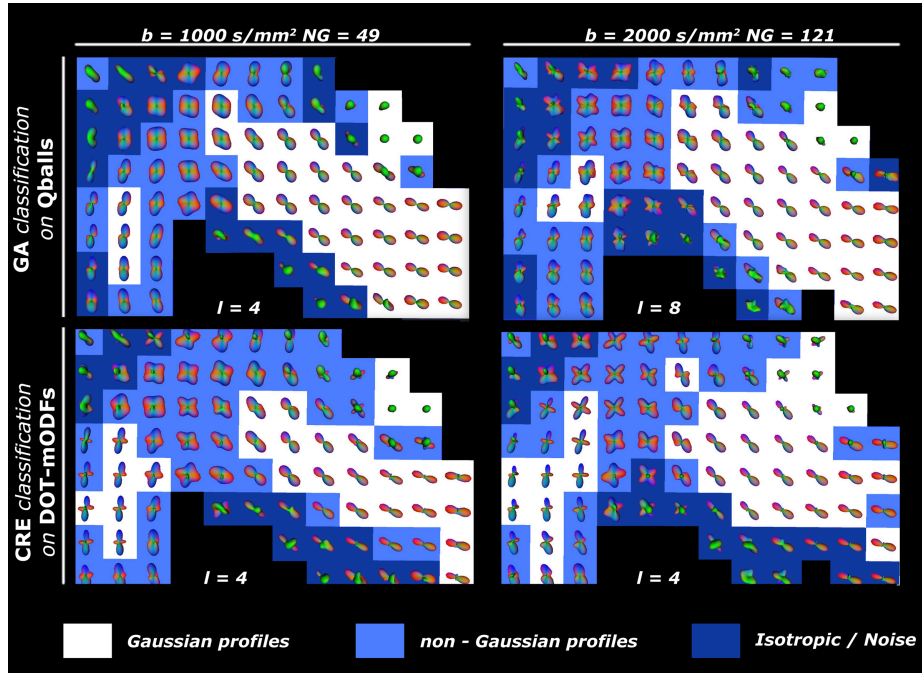


Fig. 4. Some examples from different classification

As an example of possible application of our classification, in Figure 5 we show hybrid visualization of the simplified data (labeling provided by GA classification) from an *in-vivo* dataset represented with 8<sup>th</sup> order CSD [12] in the non-Gaussian classified regions, and DTI ODFs in the Gaussian regions. The difference in running time is as follows: computing CSD of order 8 for the whole brain in white matter mask: 540 minutes (36601 voxels). Computing CSD of order 8 in labeled crossing : 120 minutes(8164 voxels). Computing DTI ODFs in labeled linear : 19 seconds<sup>2</sup>. With hybrid data modeling there is nearly a factor 5 gain in computation compared to modeling full brain data with the same high order model. Also interaction in the visualization pipeline becomes possible, even for a full brain slice.

## 4 Discussion & Conclusions

Finding the correct threshold for classification, in real data is important for accurate classification, and most of the times depends on the b-value from the acquisition protocol and the angular configuration. In our study, the thresholds found in the 90° phantom configuration were very similar to the thresholds used to classify the real data at the same b-value. Therefore, they can be of

<sup>2</sup> These times were calculated on a 1.66 GHz processor dual core Intel machine with 2 GB of RAM. The time can be improved by parallelizing the code and changing the parameters of CSD regularization.

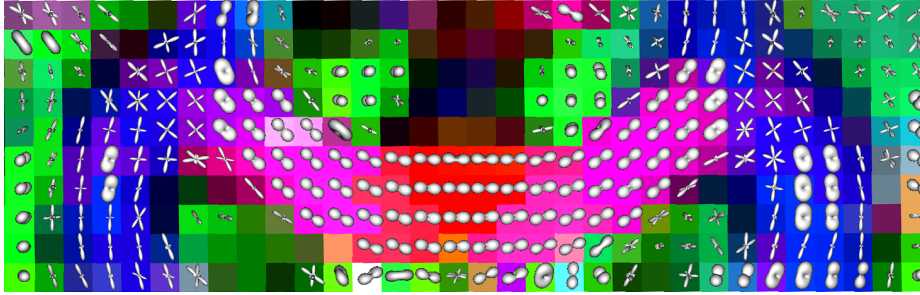


**Fig. 5.** Example of hybrid visualization of CSD [12] and DTI ODFs.

great importance for post-processing clinically acquired data. For *in-vivo* data, a semi-automatic detection of thresholds, with feedback from the user identifying positive and negative examples can be very useful to set the classification thresholds.

There are few important messages from this work. Denoising as a pre-processing step improves the coherence of the classification areas and enhances the HARDI profiles. ADC and QBall demonstrate strong classification information, even though sometimes lack sufficient angular resolution for small crossing angle discrimination. The sharper and slightly more noisy profiles produced by DOT and its derivation (we believe this would be the case for SD techniques [6] as well) find more accurate number of maxima and are better suited for fiber tracking applications. Increasing the acquisition parameters (b-value  $> 2000s/mm^2$  and  $NG > 80$ ) as well as model order, does not significantly improve the classification power. In contrary, the high b-value acquisitions produce low SNR datasets that are worse for classification, and result in polluted HARDI profiles. It is even doubtful if, in practice, these higher b-value datasets improve fiber tracking.

In this work, we investigated a broad range of different anisotropy measures proposed in the literature and applied them as classification criteria for discriminating different fiber configurations within the white matter. All the measures were applied on the HARDI reconstructions and, except for CRE and NM, all measures are directly implemented on SH representation of the model that can be calculated and thresholded in real time. Some of the measures such as GA, GFA and CRE behave in similar fashion and are relatively good classification criteria. Others, such as FMI, R2, Ri, Shannon entropy, are highly dependent on the acquisition parameters and the angular configuration of the profiles, and therefore, are less reliable in clinical settings. The NM measure belongs to a different category of measures because it does not need a thresholding process for classification. However, it is very dependent on the HARDI profile and can produce many false positives in the presence of noise. A strong message that comes out of this work, is that the measures can be applied on different SPFs and still have the same classification power (especially in the case of ADC and QBall). This means that the users can use any existing HARDI modeling technique and apply classification measures to distinguish between Gaussian and non-Gaussian profiles. If the non-Gaussian voxels are correctly classified in a first step, one can ignore all the other single fiber voxels and properly focus on the

modeling and more accurate reconstruction of these voxels. Hence, as a second step, one can use a complex modeling approach, such as SD, PAS-MRI [18], etc. In clinical settings, the simplification of the data into Gaussian and non-Gaussian areas can be desired and presents a new contrast as such, even though complex structures are oversimplified as non-Gaussian. It can lead to new ways to study the white matter.

Future work will address combination of different measures for better reliability of the classified regions. Comparison of our simple and fast classification with some of the existing classification schemes as in the work of Schnell et al. [19] or learning approach such as boosting on the entire set of measures to statistically determine the discriminative strength of each feature, is addressed as future work as well. However these approaches are not interactive and real-time and the comparison should be done for validation purposes of our method only.

Nonetheless, we showed that reliable classification of Gaussian and non-Gaussian profiles can be done with some of the existing measures. The data can therefore be simplified into linear, crossing and isotropic/noise voxels. This means that more sophisticated hybrid methods, which are more time consuming can be applied only in the non-Gaussian areas, whereas linear and isotropic areas can be modeled with a simple diffusion tensor ODFs (Figure 5). This has a huge potential in the employment of the HARDI techniques in a clinical settings and enabling moderate post-processing time. Another application of the classification information can be in visualizing uncertainties in fiber tracking algorithms by attributing transparency on the unreliable fiber tracts.

## 5 Acknowledgements

We thank Alard Roebroek from Maastricht Brain Imaging Center, Department of Cognitive Neuroscience, Faculty of Psychology, Maastricht University, The Netherlands and Pim Pullens from Brain Innovation B.V., Maastricht, The Netherlands for providing us with in-vivo datasets. This study was financially supported by the VENI program of the Netherlands Organization for Scientific Research NWO (Anna Vilanova) and by the Netherlands Organization for Scientific Research (NWO), project number 643.100.503 MFMV (Vesna Prčkovska).

## References

1. Basser, P.J., Mattiello, J., Lebihan, D.: MR diffusion tensor spectroscopy and imaging. *Biophys. J.* **66**(1) (January 1994) 259–267
2. Frank, L.R.: Characterization of anisotropy in high angular resolution diffusion-weighted mri. *Magn Reson Med* **47**(6) (2002) 1083–99
3. Alexander, D.C., Barker, G.J., Arridge, S.R.: Detection and modeling of non-gaussian apparent diffusion coefficient profiles in human brain data. *Magn Reson Med* **48**(2) (2002) 331–40
4. Tuch, D.: Q-ball imaging. *Magn Reson Med* **52** (2004) 1358–1372
5. Özarslan, E., Shepherd, T.M., Vemuri, B.C., Blackband, S.J., Mareci, T.H.: Resolution of complex tissue microarchitecture using the diffusion orientation transform (DOT). *NeuroImage* **36**(3) (July 2006) 1086–1103

6. Jian, B., Vemuri, B.C.: A unified computational framework for deconvolution to reconstruct multiple fibers from Diffusion Weighted MRI. *IEEE Transactions on Medical Imaging* **26**(11) (2007) 1464–1471
7. Rao, M., Chen, Y., Vemuri, B.C., Wang, F.: Cumulative residual entropy: A new measure of information. *IEEE Transactions on Information Theory* **50**(6) (June 2004) 1220–1228
8. Chen, Y., Guo, W., Zeng, Q., Yan, X., Rao, M., Liu, Y.: Apparent diffusion coefficient approximation and diffusion anisotropy characterization in DWI. In: *Information Processing in Medical Imaging*. (2005) 246–257
9. Descoteaux, M., Angelino, E., Fitzgibbons, S., Deriche, R.: Apparent diffusion coefficients from high angular resolution diffusion imaging: Estimation and applications. *Magn Reson in Med* **56** (2006) 395–410
10. Özarıslan, E., Vemuri, B.C., Mareci, T.H.: Generalized scalar measures for diffusion MRI using trace, variance, and entropy. *Magn Reson Med* **53**(4) (2005) 866–76
11. Leow, A., Zhu, S., Zhan, L., McMahon, K., de Zubicaray, G., Meredith, M., Wright, M., Thompson, P.: A study of information gain in high angular resolution diffusion imaging (HARDI). In: *Computational Diffusion MRI Workshop, MICCAI*. (2008)
12. Tournier, J.D., Calamante, F., Connelly, A.: Robust determination of the fibre orientation distribution in diffusion MRI: non-negativity constrained super-resolved spherical deconvolution. *Neuroimage* **35**(4) (2007) 1459–72
13. Descoteaux, M., Angelino, E., Fitzgibbons, S., Deriche, R.: Regularized, fast and robust analytical q-ball imaging. *Magn Reson Med* **58** (2007) 497–510
14. Wedeen, V.J., Hagmann, P., Tseng, W.Y., Reese, T.G., Weisskoff, R.M.: Mapping complex tissue architecture with diffusion spectrum magnetic resonance imaging. *Magn Reson Med* **54**(6) (2005) 1377–1386
15. Poupon, C., Rieul, B., Kezele, I., Perrin, M., Poupon, F., Mangin, J.F.: New diffusion phantoms dedicated to the study and validation of HARDI models. *Magn Reson in Med* **60** (2008) 1276–1283
16. Descoteaux, M., Wiest-Daesslé, N., Prima, S., Barillot, C., Deriche, R.: Impact of Rician Adapted Non-Local Means Filtering on HARDI. In: *MICCAI*. Volume 5242. (2008) 122–130
17. Prčkovska, V., Roebroek, A.F., Pullens, W., Vilanova, A., ter Haar Romeny, B.M.: Optimal acquisition schemes in high angular resolution diffusion weighted imaging. In: *MICCAI*. Volume 5242 of LNCS., Springer (2008) 9–17
18. Jansons, K.M., Alexander, D.: Persistent angular structure: new insights from diffusion magnetic resonance imaging data. *Inverse Problems* **19** (2003) 1031–1046
19. Schnell, S., Saur, D., Kreher, B., Hennig, J., Burkhardt, H., Kiselev, V.: Fully automated classification of HARDI in vivo data using a support vector machine. *NeuroImage* **46**(3) (2009) 642 – 651